EUROPEAN ORGANIZATION FOR NUCLEAR RESEARCH (CERN)

CERN-EP-2017-254
LHCb-PAPER-2017-037
13 October 2015

Measurement of the $B^{\pm}$ production cross-section in pp collisions at $\sqrt{s} = 7$ and 13 TeV

LHCb collaboration†

Abstract

The production of $B^{\pm}$ mesons is studied in pp collisions at centre-of-mass energies of 7 and 13 TeV, using $B^{\pm} \to J/\psi K^{\pm}$ decays and data samples corresponding to $1.0\,\mathrm{fb}^{-1}$ and $0.3\,\mathrm{fb}^{-1}$, respectively. The production cross-sections summed over both charges and integrated over the transverse momentum range $0 < p_{\mathrm{T}} < 40\,\mathrm{GeV}/c$ and the rapidity range $2.0 < y < 4.5$ are measured to be

$$\sigma(pp \to B^{\pm}X, \sqrt{s} = \ \ 7\,\mathrm{TeV}) = 43.0 \pm 0.2 \pm 2.5 \pm 1.7\,\mu\mathrm{b},$$
$$\sigma(pp \to B^{\pm}X, \sqrt{s} = 13\,\mathrm{TeV}) = 86.6 \pm 0.5 \pm 5.4 \pm 3.4\,\mu\mathrm{b},$$

where the first uncertainties are statistical, the second are systematic, and the third are due to the limited knowledge of the $B^{\pm} \to J/\psi K^{\pm}$ branching fraction. The ratio of the cross-section at 13 TeV to that at 7 TeV is determined to be $2.02 \pm 0.02\,(\mathrm{stat}) \pm 0.12\,(\mathrm{syst})$. Differential cross-sections are also reported as functions of p_{T} and y. All results are in agreement with theoretical calculations based on the state-of-art fixed next-to-leading order quantum chromodynamics.

Submitted to JHEP

†Authors are listed at the end of this paper.

1 Introduction

Precise measurements of the production cross-section of $B^{\pm}$ mesons in pp collisions provide important tests of perturbative quantum chromodynamics (QCD) calculations, particularly of the state-of-the-art calculations based on the fixed next-to-leading order QCD with next-to-leading logarithm large transverse momentum resummation (FONLL) approach [1, 2]. The FONLL predictions have large uncertainties arising from the choices of the renormalisation and factorisation scales, and from the b-quark mass. Measurements of the integrated and differential cross-sections can test the validity of these choices. The ratio of cross-sections between different centre-of-mass energies is of particular interest due to cancellations that occur in the theoretical and experimental uncertainties.

Previous measurements of $B^{\pm}$ production have been performed in different kinematic regions at the centre-of-mass energy $\sqrt{s} = 7\,\text{TeV}$ by several experiments at the Large Hadron Collider. The CMS collaboration reported the integrated and differential $B^{\pm}$ production cross-sections in the range $p_{\mathrm{T}} > 5\,\text{GeV}/c$ and $|y| < 2.4$ [3, 4], where p_{T} and y are the component of the momentum transverse to the beam line and the rapidity of the $B^{\pm}$ mesons, respectively. The ATLAS collaboration measured the production cross-sections in the range $9 < p_{\mathrm{T}} < 120\,\text{GeV}/c$ and $|y| < 2.25$ [5]. The LHCb collaboration measured the integrated and differential cross-sections for $B^{\pm}$ with $0 < p_{\mathrm{T}} < 40\,\text{GeV}/c$ and $2.0 < y < 4.5$ using a data sample collected in 2010 that corresponds to an integrated luminosity of $35\,\text{pb}^{-1}$ [6]. This result was later updated using a data sample collected in early 2011, corresponding to an integrated luminosity of $362\,\text{pb}^{-1}$ [7].

This article updates the previous LHCb results using a larger data sample collected in 2011 with the LHCb experiment at $\sqrt{s} = 7\,\text{TeV}$ and corresponding to an integrated luminosity of $1.0\,\text{fb}^{-1}$. The first measurements of the integrated and differential cross-sections of $B^{\pm}$ mesons at $\sqrt{s} = 13\,\text{TeV}$ are also presented, using a data sample collected in 2015 and corresponding to an integrated luminosity of $0.3\,\text{fb}^{-1}$. Following the previous LHCb measurements [6, 7], the $B^{\pm}$ mesons are reconstructed in the $B^{\pm} \to J/\psi K^{\pm}$ mode followed by $J/\psi \to \mu^{+}\mu^{-}$ and the production cross-sections are measured in the range $0 < p_{\mathrm{T}} < 40\,\text{GeV}/c$ and $2.0 < y < 4.5$. The ratio of the cross-sections in the 13 TeV and 7 TeV data is also measured as a function of p_{T} and y.

2 Event selection

The LHCb detector [8, 9] is a single-arm forward spectrometer covering the pseudorapidity range $2 < \eta < 5$, designed for the study of particles containing b or c quarks. The detector includes a high-precision tracking system consisting of a silicon-strip vertex detector surrounding the pp interaction region, a large-area silicon-strip detector located upstream of a dipole magnet with a bending power of about 4 Tm, and three stations of silicon-strip detectors and straw drift tubes placed downstream of the magnet. The tracking system provides a measurement of momentum, p, of charged particles with a relative uncertainty that varies from 0.5% at low momentum to 1.0% at 200 GeV/c. The minimum distance of a track to a primary vertex, the impact parameter, is measured with a resolution of $(15 + 29/p_{\mathrm{T}})\,\mu\text{m}$, where p_{T} is in units of GeV/c. Different types of charged hadrons are distinguished using information from two ring-imaging Cherenkov detectors. Photons, electrons and hadrons are identified by a calorimeter system consisting of scintillating-pad

(SPD) and preshower detectors, an electromagnetic calorimeter and a hadronic calorimeter. Muons are identified by a system composed of alternating layers of iron and multiwire proportional chambers.

The online event selection is performed by a trigger, which consists of a hardware stage (L0), based on information from the calorimeter and muon systems, followed by a two-stage software-based high-level trigger (HLT1, HLT2) [10], where the HLT1 stage uses partial event reconstruction to reduce the rate and the HLT2 stage applies a full event reconstruction. At the hardware stage, events are required to have a dimuon candidate with large p_{T}, while at the software stage the dimuon invariant mass is required to be consistent with the known J/ψ mass [11]. Finally, a set of global event cuts (GEC) is applied in order to prevent high-multiplicity events from dominating the processing time of the software trigger, which includes the requirement that the number of hits in the SPD subdetector should be less than 900.

Simulated events are used to optimise the selection, determine some of the efficiencies and estimate the background contamination. The simulation is based on the PYTHIA8 generator [12] with a specific LHCb configuration [13]. Decays of hadrons are described by EVTGEN [14], in which final-state radiation is generated using PHOTOS [15]. The interaction of the generated particles with the detector, and its response, are implemented using the GEANT4 toolkit [16], as described in Ref. [17].

The $B^{\pm}$ candidates are made by combining J/ψ and $K^{\pm}$ candidates. The offline event selection forms J/ψ candidates using pairs of muons with opposite charge. The muon candidates must have $p_{\mathrm{T}} > 700\,\mathrm{MeV}/c$, and satisfy track-reconstruction quality and particle identification (PID) requirements. The muon pair is required to be consistent with originating from a common vertex [18] and have an invariant mass, $M(\mu\mu)$, within the range $3.04 < M(\mu\mu) < 3.14\,\mathrm{GeV}/c^2$. The $K^{\pm}$ candidates are required to have p_{T} greater than $500\,\mathrm{MeV}/c$ and satisfy track-reconstruction quality requirements. No PID requirement is applied to select the kaon, as the only topologically similar decay, $B^{\pm} \to J/\psi\,\pi^{\pm}$, is Cabibbo suppressed.

The three tracks in the final state of the $B^{\pm}$ decay are required to form a common vertex with a good vertex-fit quality. In order to suppress background due to the random combination of particles produced in the pp interactions, the $B^{\pm}$ candidates are required to have a decay time larger than 0.3 ps. Finally, $B^{\pm}$ candidates with $0 < p_{\mathrm{T}} < 40\,\mathrm{GeV}/c$ and $2.0 < y < 4.5$ are selected for subsequent analysis.

3 Cross-section determination

The differential production cross-section of $B^{\pm}$ mesons is measured as a function of p_{T} and y using

$$\frac{\mathrm{d}^2\sigma}{\mathrm{d}y\mathrm{d}p_{\mathrm{T}}} = \frac{N_{B^{\pm}}}{\mathcal{L} \times \varepsilon_{\mathrm{Tot}} \times \mathcal{B}\left(B^{\pm} \to J/\psi\, K^{\pm}\right) \times \mathcal{B}\left(J/\psi \to \mu^+\mu^-\right) \times \Delta y \times \Delta p_{\mathrm{T}}}, \tag{1}$$

where $N_{B^{\pm}}$ is the number of reconstructed $B^{\pm} \to J/\psi\, K^{\pm}$ candidates in a given (p_{T}, y) bin after background subtraction, $\mathcal{L}$ is the integrated luminosity, $\varepsilon_{\mathrm{Tot}}$ is the bin-dependent total efficiency, $\mathcal{B}\left(B^{\pm} \to J/\psi\, K^{\pm}\right)$ is the branching fraction of $B^{\pm}$ decays to $J/\psi\, K^{\pm}$ [19, 20], $\mathcal{B}\left(J/\psi \to \mu^+\mu^-\right)$ is the branching fraction of J/ψ decays to $\mu^+\mu^-$ [11], and Δy and Δp_{T} are the bin widths in y and p_{T}. The value of $\mathcal{B}\left(B^{\pm} \to J/\psi\, K^{\pm}\right)$ is calculated

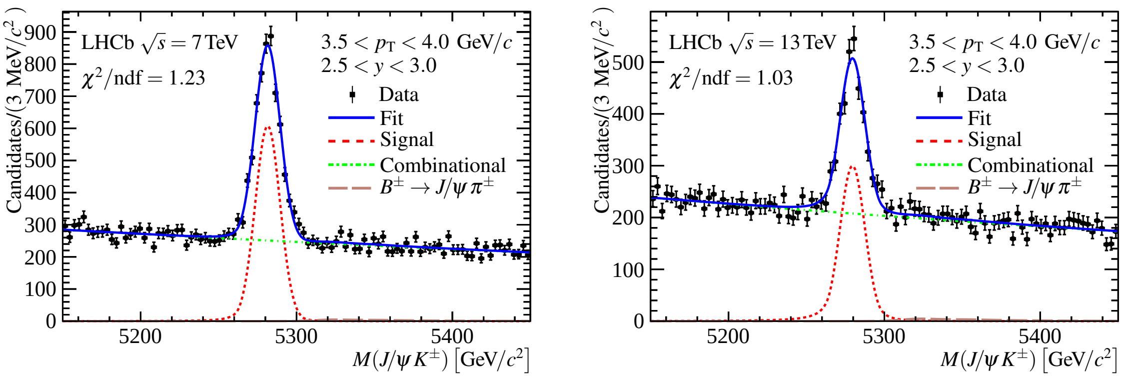

Figure 1: Invariant mass distributions of $B^{\pm}$ candidates in the range $3.5 < p_{\mathrm{T}} < 4.0\,\mathrm{GeV}/c$ and $2.5 < y < 3.0$ using (left) 7 TeV and (right) 13 TeV data. The black points are the number of selected candidates in each bin, the blue curve represents the fit result, the red-dotted line represents the $B^{\pm} \to J/\psi\, K^{\pm}$ signal, and the green- and brown-dashed lines are contributions from the combinatorial and the Cabibbo-suppressed backgrounds. The Cabibbo-suppressed background contribution $B^{\pm} \to J/\psi\, \pi^{\pm}$ is only just visible at masses above the signal peak.

to be $(1.044 \pm 0.040) \times 10^{-3}$ by combining the two exclusive measurements from the Belle [19] and BaBar [20] collaborations, under the assumption that only the uncertainty for $J/\psi \to \mu^{+}\mu^{-}$ branching fraction is correlated.

The yield of $B^{\pm} \to J/\psi\, K^{\pm}$ decays in each $(p_{\mathrm{T}},\, y)$ bin is obtained independently by fitting the invariant mass distribution of the $B^{\pm}$ candidates, $M(J/\psi\, K^{\pm})$, in the interval $5150 < M(J/\psi\, K^{\pm}) < 5450\,\mathrm{MeV}/c^2$, using an extended unbinned maximum likelihood fit. The $M(J/\psi\, K^{\pm})$ distribution is described by a probability density function (PDF) consisting of the following three components: a modified Crystal Ball (CB) function [21] to model the signal, an exponential function to model the combinatorial background, and a double CB function to model the contamination from the Cabibbo suppressed decay $B^{\pm} \to J/\psi\, \pi^{\pm}$, where the charged pion is misidentified as a kaon. The modified CB function used for the signal component has tails on both the low- and the high-mass side of the peak, which are described by separate parameters. In each bin, the tail parameters are determined from simulation, leaving the mean and width as free parameters. The shape of the misidentification background is obtained using simulated $B^{\pm} \to J/\psi\, \pi^{\pm}$ decays that satisfy the selection criteria for the decay $B^{\pm} \to J/\psi\, K^{\pm}$, and the yield of the misidentification background is determined according to the branching fraction ratio $\mathcal{B}(B^{\pm} \to J/\psi\, \pi^{\pm})/\mathcal{B}(B^{\pm} \to J/\psi\, K^{\pm})$ from Ref. [11]. Figure 1 shows, as an example, the invariant mass distribution of the $B^{\pm}$ candidates in the range $3.5 < p_{\mathrm{T}} < 4.0\,\mathrm{GeV}/c$ and $2.5 < y < 3.0$.

The total efficiency, $\varepsilon_{\mathrm{tot}}$, is the product of several efficiencies and can be written as

$$\varepsilon_{\mathrm{tot}} = \varepsilon_{\mathrm{acc}} \times \varepsilon_{\mathrm{reco\&sel}} \times \varepsilon_{\mathrm{PID}} \times \varepsilon_{\mathrm{track}} \times \varepsilon_{\mathrm{trigger}} \times \varepsilon_{\mathrm{GEC}}\,. \tag{2}$$

The acceptance factor, $\varepsilon_{\mathrm{acc}}$, is the fraction of signal with all final-state particles within the fiducial region of the detector acceptance, and is calculated from simulation. The efficiency of the particle reconstruction and event selection, $\varepsilon_{\mathrm{reco\&sel}}$, is also determined from simulation. The efficiency of identifying the two muons in the final state, $\varepsilon_{\mathrm{PID}}$, and the track finding efficiency, $\varepsilon_{\mathrm{track}}$, are measured using a tag-and-probe method [22, 23] on

Table 1: Summary of relative systematic uncertainties on the integrated production cross-sections at $\sqrt{s}=7$ and $13\,\text{TeV}$, and the ratio of the cross-sections $R(13\,\text{TeV}/7\,\text{TeV})$.

Sources	Uncertainty (%)		
	7 TeV	13 TeV	$R(13\,\text{TeV}/7\,\text{TeV})$
Luminosity	1.7	3.9	3.4
Branching fractions	4.1	4.1	0.0
Binning	2.6	2.7	0.0
Mass fits	2.7	1.3	1.5
Acceptance	0.2	0.1	0.2
Reconstruction	0.1	0.1	0.2
Track	1.6	2.6	1.0
PID	0.4	0.1	0.4
Trigger	3.5	2.6	4.4
GEC	0.7	0.7	1.0
Selection	1.0	1.1	0.1
Weighting	0.2	0.2	0.3
Total	7.1	7.4	5.9

a control data sample of $J/\psi \to \mu^+\mu^-$ decays. The trigger efficiency, $\varepsilon_{\text{trigger}}$, is estimated in two parts, which are $\varepsilon_{\text{L0\&HLT1}}$ and $\varepsilon_{\text{HLT2}}$. The $\varepsilon_{\text{L0\&HLT1}}$ efficiency is evaluated by estimating the fraction of events in a trigger-unbiased data sample that satisfy the trigger requirements, and the $\varepsilon_{\text{HLT2}}$ efficiency is evaluated using simulated signal events, as the effects of HLT2 trigger are well modelled. The GEC efficiency, ε_{GEC}, is measured to be $(99.2 \pm 0.1)\%$ for the 7 TeV and $(99.3 \pm 0.1)\%$ for the 13 TeV data sample, and is independent of p_{T} and y. It is extracted by fitting the SPD multiplicity distribution and extrapolating the function to determine the fraction of events that are accepted.

4 Systematic uncertainties

Sources of systematic uncertainty associated with the determination of the luminosity, branching fractions, signal yields, efficiencies, along with their effects on the integrated cross-section measurements, are summarised in Table 1. The total systematic uncertainty is obtained from the sum in quadrature of all contributions. Several uncertainties have been reduced in the $\sqrt{s}=13\,\text{TeV}$ measurement, due to a larger simulation sample and a better understanding of the efficiency.

Following the procedures used in Ref. [24], the relative uncertainty on the luminosity is determined to be 1.7% for the 7 TeV data and 3.9% for the 13 TeV data sample. The relative uncertainty on $\mathcal{B}\,(B^\pm \to J/\psi\,K^\pm)$ is 4.1% [19, 20], while the uncertainty on $\mathcal{B}\,(J/\psi \to \mu^+\mu^-)$ [11] is negligible.

The variation of the efficiency within a bin induces an uncertainty if the kinematic distributions of the simulated samples do not match those of the data. This uncertainty, which is important close to the edges of the fiducial region, is estimated by increasing or decreasing the bin width in p_{T} and y by a factor of two. The largest variation of the integrated cross-section measurement is taken as a systematic uncertainty on the production cross-sections.

The systematic uncertainty associated with the invariant mass fits is obtained by performing fits using alternative choices for the signal and background PDFs. The signal PDF is replaced by a HYPATIA function [25], while the combinatorial background model is modified to be either a first-order or second-order polynomial function. The largest resulting variation of the cross-section measurement is taken as a systematic uncertainty.

The efficiencies of the tracking, PID and trigger are estimated using control samples, and systematic uncertainties arise due to the limited sample sizes. An additional uncertainty arises on the track-reconstruction efficiency due to limited knowledge of the material budget of the detector, which induces a 1.1% uncertainty on the kaon reconstruction efficiency due to modelling of hadronic interactions with the detector material. There is an additional systematic uncertainty on the tracking efficiency from the method [23], which amounts to 0.4% (0.8%) at 7 TeV (13 TeV). For the uncertainty from the PID efficiency, the binning effect is studied by enlarging or decreasing the number of bins by a factor of two in the calculation of the PID efficiency, and taking the largest deviation from the default as the uncertainty. An additional uncertainty on the trigger efficiency is determined by testing the procedure in simulation and taking the deviation as the systematic uncertainty.

The GEC efficiency is obtained from data, and the inefficiency of the global event cuts is taken as a systematic uncertainty. The uncertainty on the offline event selection efficiencies are estimated from data and simulation by varying the selection criteria, comparing the ratios of the selection and reconstruction efficiencies between data and simulation, and taking the largest deviation as the systematic uncertainty.

A weighting procedure is applied to the simulation sample to correct for discrepancies between data and simulation in the track multiplicities. The weighting factors of the simulated events are varied within their statistical uncertainties and the largest deviation of the measured cross-section is taken as a systematic uncertainty.

5 Results

The measured $B^{\pm}$ meson production cross-sections for the 7 TeV and 13 TeV data in the range $0 < p_{\mathrm{T}} < 40\,\mathrm{GeV}/c$ and $2.0 < y < 4.5$ are

$$\sigma(pp \to B^{\pm}X, \sqrt{s} = 7\,\mathrm{TeV}) = 43.0 \pm 0.2 \pm 2.5 \pm 1.7\,\mu\mathrm{b},$$
$$\sigma(pp \to B^{\pm}X, \sqrt{s} = 13\,\mathrm{TeV}) = 86.6 \pm 0.5 \pm 5.4 \pm 3.4\,\mu\mathrm{b},$$

where the first uncertainties are statistical, the second are systematic, and the third are due to the limited knowledge of the $B^{\pm} \to J/\psi\, K^{\pm}$ branching fraction. The measured double-differential cross-sections at 7 TeV and 13 TeV as functions of p_{T} and y are shown in Fig. 2, where the measurements are compared with theoretical predictions based on FONLL calculations [26]. The corresponding single-differential cross-sections are shown in Figs. 3 and 4. The single-differential cross-sections and the production cross-section in the above range of p_{T} and y are calculated from the measured double-differential cross-sections. All results are in agreement with the FONLL predictions. The results are tabulated in Appendix A.

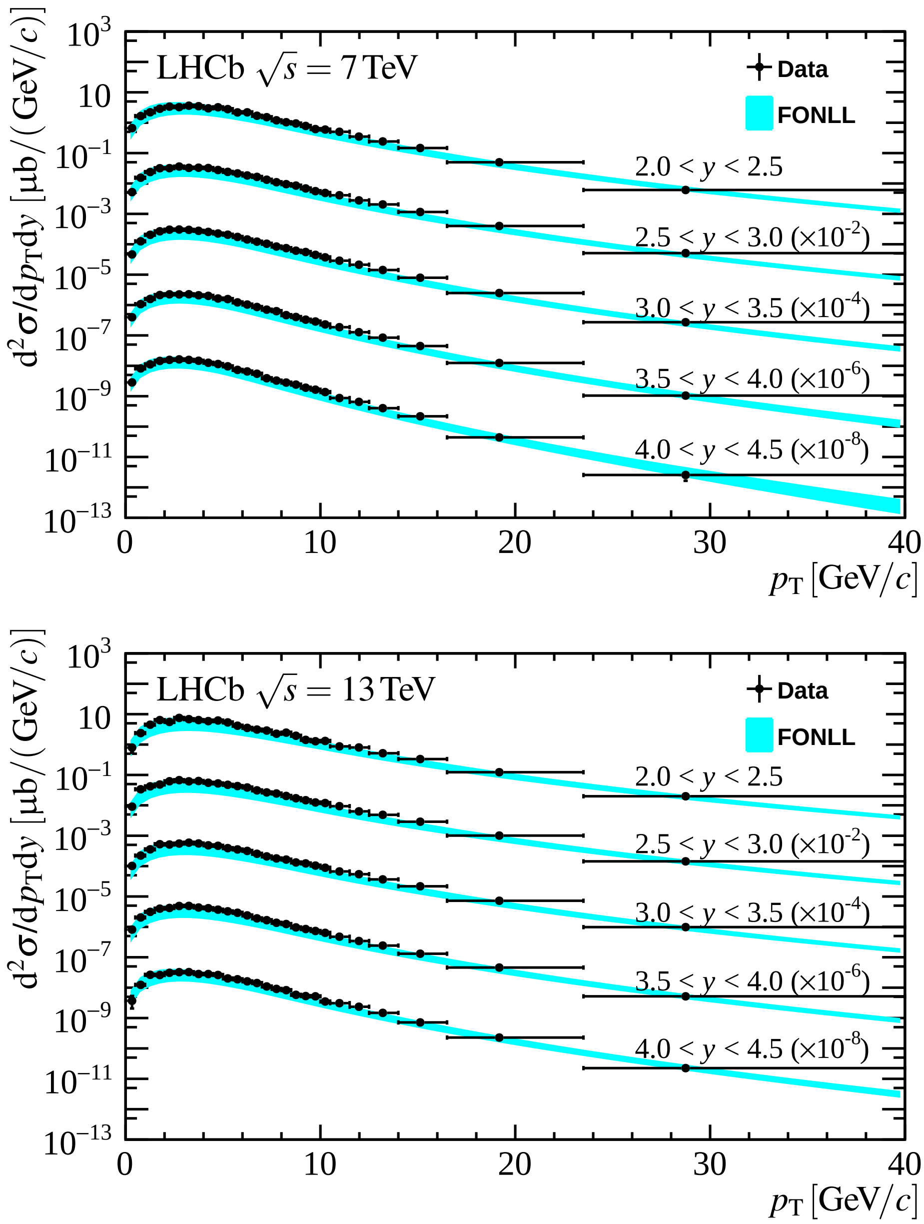

Figure 2: Measured $B^{\pm}$ double-differential production cross-sections at (top) 7 TeV and (bottom) 13 TeV as a function of p_T and y. The black points represent the measured values, and the cyan bands are the FONLL predictions [26]. Each set of measurements and predictions in a given rapidity bin is offset by a multiplicative factor 10^{-m}, where the offset factor is shown after the rapidity range. The error bars include both the statistical and systematic uncertainties.

The ratio of the cross-section at 13 TeV to that at 7 TeV, $R(13\,\text{TeV}/7\,\text{TeV})$, is determined to be

$$R(13\,\text{TeV}/7\,\text{TeV}) = 2.02 \pm 0.02\,(\text{stat}) \pm 0.12\,(\text{syst})\,.$$

In the ratio calculation, the systematic uncertainties on the luminosities at 13 and 7 TeV are taken to be 50% correlated, as in Ref. [24]; the systematic uncertainties associated with the branching fractions, mass fits, event selection and binning are assumed to be

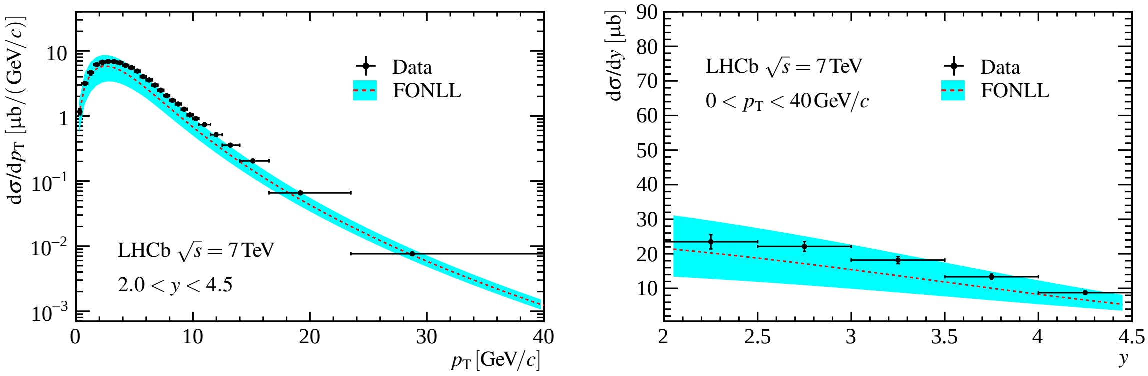

Figure 3: Measured $B^{\pm}$ differential cross-section at 7 TeV as a function of (left) p_{T} or (right) y. The black points represent the measured values, the red-dashed line and cyan band represent the central values and uncertainties of the FONLL prediction [26]. The error bars include both the statistical and systematic uncertainties.

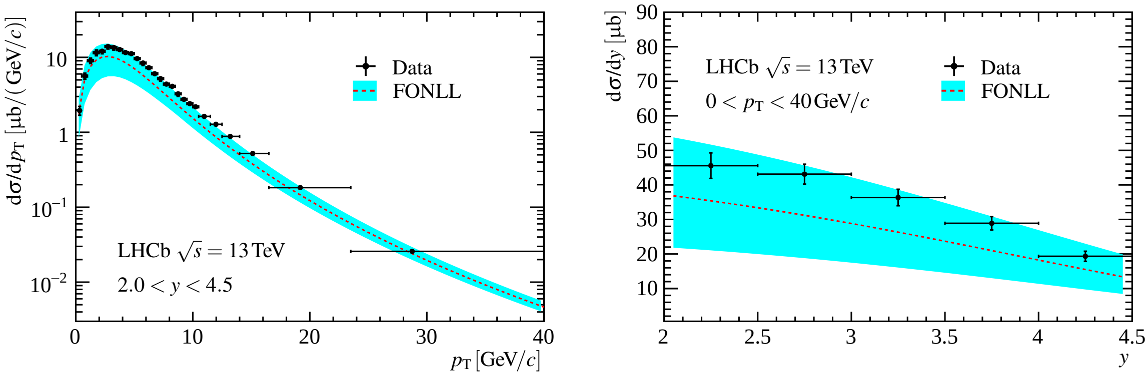

Figure 4: Measured $B^{\pm}$ differential cross-section at 13 TeV as a function of (left) p_{T} or (right) y. The black points represent the measured values, the red-dashed line and cyan band represent the central values and uncertainties of the FONLL prediction [26]. The error bars include both the statistical and systematic uncertainties.

completely correlated; and all other uncertainties are considered to be uncorrelated. The systematic uncertainty on R is summarised in Table 1. In Fig. 5, the ratio of the cross-section at 13 TeV to that at 7 TeV as a function of p_{T} or y is compared with the FONLL predictions. The measured results agree with the FONLL predictions in both the shape and the scale.

6 Summary

In summary, the double-differential production cross-sections of $B^{\pm}$ mesons are measured as functions of the transverse momentum and rapidity, using pp collision data collected with the LHCb detector at the Large Hadron Collider. The integrated luminosities of the data samples are $1.0\,\mathrm{fb}^{-1}$ and $0.3\,\mathrm{fb}^{-1}$ at the centre-of-mass energies of 7 TeV and 13 TeV, respectively. The measurements are performed in the transverse momentum range

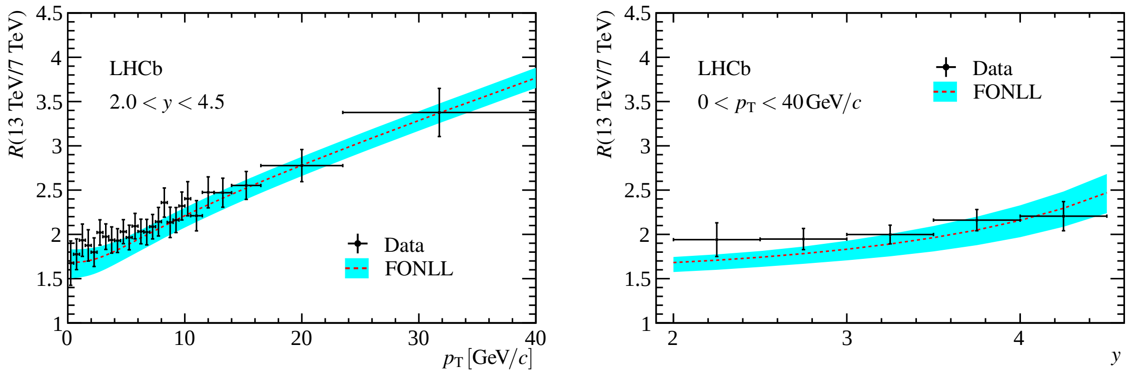

Figure 5: Ratio of the $B^{\pm}$ cross-section at 13 TeV to that at 7 TeV as a function of (left) p_{T} or (right) y. The black points represent the measured values, the red-dashed line and cyan band represent the central values and uncertainties of the FONLL prediction [26].

$0 < p_{\mathrm{T}} < 40\,\mathrm{GeV}/c$ and the rapidity range $2.0 < y < 4.5$. The 7 TeV results are consistent with previously published results [6, 7], with improved precision in the low y region. This measurement supersedes previous results. The ratio of the production cross-section at 13 TeV to that at 7 TeV is also measured. All results are in agreement with theoretical calculations based on the FONLL approach.

Acknowledgements

We express our gratitude to our colleagues in the CERN accelerator departments for the excellent performance of the LHC. We thank the technical and administrative staff at the LHCb institutes. We acknowledge support from CERN and from the national agencies: CAPES, CNPq, FAPERJ and FINEP (Brazil); MOST and NSFC (China); CNRS/IN2P3 (France); BMBF, DFG and MPG (Germany); INFN (Italy); NWO (The Netherlands); MNiSW and NCN (Poland); MEN/IFA (Romania); MinES and FASO (Russia); MinECo (Spain); SNSF and SER (Switzerland); NASU (Ukraine); STFC (United Kingdom); NSF (USA). We acknowledge the computing resources that are provided by CERN, IN2P3 (France), KIT and DESY (Germany), INFN (Italy), SURF (The Netherlands), PIC (Spain), GridPP (United Kingdom), RRCKI and Yandex LLC (Russia), CSCS (Switzerland), IFIN-HH (Romania), CBPF (Brazil), PL-GRID (Poland) and OSC (USA). We are indebted to the communities behind the multiple open-source software packages on which we depend. Individual groups or members have received support from AvH Foundation (Germany), EPLANET, Marie Skłodowska-Curie Actions and ERC (European Union), ANR, Labex P2IO, ENIGMASS and OCEVU, and Région Auvergne-Rhône-Alpes (France), RFBR and Yandex LLC (Russia), GVA, XuntaGal and GENCAT (Spain), Herchel Smith Fund, the Royal Society, the English-Speaking Union and the Leverhulme Trust (United Kingdom).

A Tabulated results

The measured $B^{\pm}$ double-differential cross-section in bins of p_{T} and y is given in Tables 2 and 3 for 7 TeV data, and Tables 4 and 5 for 13 TeV data. The measured $B^{\pm}$ single-differential cross-section as a function of p_{T} or y is given in Tables 6 and 7, respectively. The limited size of the simulation samples gives relative systematic uncertainties in the high p_{T} region that are larger than those in the low p_{T} region.

Table 2: Measured $B^{\pm}$ double-differential cross-section (in units of nb) at 7 TeV, as a function of p_{T} and y, in the rapidity regions of $2.0 < y < 2.5$, $2.5 < y < 3.0$, and $3.0 < y < 3.5$.

p_{T} [GeV/c]	$2.0 < y < 2.5$	$2.5 < y < 3.0$	$3.0 < y < 3.5$
0.0 – 0.5	664.5±103.3± 99.9	519.8±35.0± 50.3	462.6±30.4± 37.5
0.5 – 1.0	1652.9±160.9±180.6	1544.9±59.8±142.0	1248.8±51.6± 94.4
1.0 – 1.5	2204.8±171.7±345.8	2381.1±71.0±212.8	2046.2±62.4±147.1
1.5 – 2.0	2879.5±191.3±311.6	3175.6±76.2±260.1	2665.7±65.1±192.5
2.0 – 2.5	3378.9±192.0±592.5	3193.0±80.1±257.7	3017.2±64.1±214.6
2.5 – 3.0	3261.7±179.8±321.9	3605.8±69.9±256.6	3056.6±60.7±220.0
3.0 – 3.5	3627.8±182.8±290.3	3263.8±66.6±263.4	2977.6±54.6±194.2
3.5 – 4.0	3491.7±175.6±419.5	3304.0±57.9±246.3	2767.2±49.8±167.7
4.0 – 4.5	2976.6±146.4±240.0	3224.0±50.9±233.4	2545.6±44.7±173.3
4.5 – 5.0	3216.9±141.1±255.9	2773.2±44.1±185.0	2258.6±39.7±134.8
5.0 – 5.5	2795.0±127.6±308.6	2408.0±41.3±158.0	2063.8±36.1±128.5
5.5 – 6.0	2183.8±101.3±160.2	2145.3±34.4±136.9	1740.5±31.3±108.4
6.0 – 6.5	2194.2± 94.8±200.1	1834.6±28.8±124.7	1437.9±27.3± 85.9
6.5 – 7.0	1694.1± 75.0±166.0	1645.1±24.4±109.0	1219.0±23.7± 69.7
7.0 – 7.5	1517.7± 65.6±102.6	1329.8±21.9± 84.9	1039.8±21.4± 59.3
7.5 – 8.0	1200.0± 54.2±134.2	1101.1±18.7± 73.8	842.3±18.1± 48.4
8.0 – 8.5	1036.9± 46.2± 91.2	950.4±16.7± 55.4	744.6±16.7± 41.3
8.5 – 9.0	943.1± 42.4±124.1	851.6±14.1± 50.5	614.3±14.9± 33.3
9.0 – 9.5	782.0± 36.7± 57.8	687.3±13.9± 39.6	554.8±13.5± 30.0
9.5 – 10.0	617.0± 30.0± 49.2	559.9±11.9± 32.8	448.5±11.9± 27.1
10.0 – 10.5	594.6± 29.4± 79.9	487.7±10.2± 26.9	371.0±10.7± 21.6
10.5 – 11.5	502.1± 17.6± 55.1	409.9± 5.9± 25.7	287.9± 6.4± 15.3
11.5 – 12.5	349.3± 13.5± 38.7	278.0± 5.0± 14.7	212.3± 5.4± 11.6
12.5 – 14.0	241.5± 8.4± 20.0	204.5± 3.1± 11.5	142.1± 3.5± 9.9
14.0 – 16.5	146.9± 4.6± 9.2	115.4± 1.7± 6.3	79.2± 2.0± 6.5
16.5 – 23.5	49.9± 1.4± 2.9	40.0± 0.5± 2.9	24.8± 0.6± 1.9
23.5 – 40.0	6.1± 0.3± 0.4	5.1± 0.1± 0.4	2.7± 0.1± 0.3

Table 3: Measured $B^{\pm}$ double-differential cross-section (in units of nb) at 7 TeV, as a function of p_{T} and y, in the rapidity regions of $3.5 < y < 4.0$ and $4.0 < y < 4.5$.

p_{T} (GeV/c)	$3.5 < y < 4.0$	$4.0 < y < 4.5$
0.0 – 0.5	396.4±29.2± 34.4	283.7±37.9± 35.3
0.5 – 1.0	1069.6±43.9± 83.6	820.5±57.0± 83.9
1.0 – 1.5	1581.2±50.0±121.1	1115.7±63.6±102.2
1.5 – 2.0	2132.1±53.8±161.0	1447.6±65.7±146.7
2.0 – 2.5	2256.6±52.1±165.1	1570.9±63.2±145.3
2.5 – 3.0	2241.9±48.6±158.9	1627.4±58.5±133.5
3.0 – 3.5	2265.2±45.6±157.5	1566.6±55.1±134.3
3.5 – 4.0	2094.9±42.2±147.0	1465.1±52.1±113.5
4.0 – 4.5	2002.0±39.2±133.4	1259.9±45.5±114.5
4.5 – 5.0	1642.0±34.0±101.1	1144.0±42.8±101.4
5.0 – 5.5	1569.5±32.0±108.9	961.9±37.0± 76.5
5.5 – 6.0	1223.2±27.2± 75.1	734.2±29.8± 73.7
6.0 – 6.5	1038.0±23.7± 62.5	652.5±27.6± 48.4
6.5 – 7.0	861.0±20.8± 53.3	548.6±24.1± 44.0
7.0 – 7.5	704.6±18.2± 40.9	390.1±19.2± 28.5
7.5 – 8.0	628.7±16.6± 37.2	326.4±17.4± 27.7
8.0 – 8.5	465.3±13.4± 28.3	280.7±15.3± 21.2
8.5 – 9.0	403.4±12.2± 22.3	241.0±13.5± 17.7
9.0 – 9.5	330.0±11.0± 20.8	190.6±11.4± 17.6
9.5 – 10.0	286.9±10.2± 17.7	163.9±10.2± 14.2
10.0 – 10.5	230.0± 8.8± 13.8	136.7± 9.5± 15.3
10.5 – 11.5	186.7± 5.4± 10.5	87.0± 4.9± 8.2
11.5 – 12.5	127.7± 4.3± 7.3	65.0± 4.0± 5.5
12.5 – 14.0	84.4± 2.8± 4.8	40.4± 2.6± 3.5
14.0 – 16.5	44.7± 1.6± 2.7	21.8± 1.4± 1.8
16.5 – 23.5	12.4± 0.5± 0.8	4.4± 0.3± 0.4
23.5 – 40.0	1.0± 0.1± 0.1	0.3± 0.1± 0.1

Table 4: Measured $B^{\pm}$ double-differential cross-section (in units of nb) at 13 TeV, as a function of p_{T} and y, in the rapidity regions of $2.0 < y < 2.5$, $2.5 < y < 3.0$, and $3.0 < y < 3.5$.

p_{T} [GeV/c]	$2.0 < y < 2.5$	$2.5 < y < 3.0$	$3.0 < y < 3.5$
0.0 – 0.5	794.4±228.1±130.0	905.7±152.4± 85.6	1013.9±183.2± 81.1
0.5 – 1.0	2384.0±362.6±322.3	3371.6±178.9±267.2	2221.2±194.6±152.5
1.0 – 1.5	4503.0±493.3±419.1	4211.5±232.8±321.1	3557.8±223.2±236.1
1.5 – 2.0	6378.3±557.8±939.8	4846.7±297.1±356.4	5255.5±236.4±370.7
2.0 – 2.5	5543.9±518.5±501.1	6186.6±236.4±465.9	5136.2±214.9±347.9
2.5 – 3.0	7517.2±555.3±695.2	6739.7±217.1±477.0	5519.8±203.8±369.2
3.0 – 3.5	6848.8±534.6±738.4	6152.6±228.5±412.6	5903.7±189.0±419.3
3.5 – 4.0	6382.6±475.5±509.5	6321.5±187.5±452.4	5560.9±167.3±368.1
4.0 – 4.5	5900.1±449.8±543.6	5525.8±162.8±371.3	4824.6±144.4±315.7
4.5 – 5.0	6185.4±412.5±503.8	5259.5±150.0±368.0	4657.9±131.8±318.8
5.0 – 5.5	5353.0±349.5±402.2	4735.5±119.4±313.3	3900.2±113.6±256.2
5.5 – 6.0	4168.6±279.7±357.4	4300.4±105.7±290.2	3535.4±101.0±245.1
6.0 – 6.5	3532.0±237.5±326.4	3865.7± 92.1±256.5	3158.4± 88.8±211.9
6.5 – 7.0	3111.7±203.9±259.2	3107.7± 77.0±227.6	2544.5± 77.0±167.0
7.0 – 7.5	2891.4±174.3±282.1	2662.1± 63.4±177.2	2086.4± 66.5±143.7
7.5 – 8.0	2270.4±149.5±182.8	2450.3± 54.9±164.1	1788.4± 58.2±122.9
8.0 – 8.5	2467.8±143.9±213.3	2034.0± 52.1±149.6	1638.5± 53.4±109.7
8.5 – 9.0	1947.3±118.9±195.0	1710.1± 44.0±118.7	1320.5± 46.2± 87.5
9.0 – 9.5	1424.4± 98.0±115.2	1472.0± 41.9± 99.1	1227.2± 42.8± 83.0
9.5 – 10.0	1283.7± 84.4± 96.4	1243.8± 36.7± 86.2	1039.0± 38.0± 74.6
10.0 – 10.5	1313.6± 78.7±100.9	1189.3± 31.3± 79.5	883.8± 34.3± 59.3
10.5 – 11.5	870.5± 43.3± 67.7	936.9± 18.1± 68.1	666.8± 20.5± 44.4
11.5 – 12.5	802.2± 38.1± 66.1	632.3± 17.1± 42.4	541.7± 17.9± 36.4
12.5 – 14.0	518.5± 22.4± 36.2	487.1± 10.1± 32.1	365.3± 11.6± 24.7
14.0 – 16.5	333.0± 12.5± 23.2	289.2± 5.8± 19.6	216.4± 6.7± 14.3
16.5 – 23.5	123.1± 4.0± 9.3	101.0± 1.8± 6.6	72.4± 2.2± 5.1
23.5 – 40.0	19.9± 0.9± 1.4	14.3± 0.4± 1.1	9.8± 0.5± 0.7

Table 5: Measured $B^{\pm}$ double-differential cross-section (in units of nb) at 13 TeV, as a function of p_{T} and y, in the rapidity regions of $3.5 < y < 4.0$ and $4.0 < y < 4.5$.

p_{T} (GeV/c)	$3.5 < y < 4.0$	$4.0 < y < 4.5$
0.0 – 0.5	814.7±111.2± 83.4	369.7±156.1± 48.4
0.5 – 1.0	2037.6±161.1±165.9	1235.7±197.9±107.4
1.0 – 1.5	3120.6±186.1±288.9	2649.3±249.5±236.6
1.5 – 2.0	3980.7±202.0±266.5	2605.7±236.3±238.8
2.0 – 2.5	4187.1±185.7±288.7	3079.7±240.3±232.1
2.5 – 3.0	4869.2±179.4±332.8	3237.0±224.2±252.6
3.0 – 3.5	4898.3±168.1±327.0	3246.0±210.9±257.8
3.5 – 4.0	4336.9±149.4±343.3	2807.4±185.1±268.8
4.0 – 4.5	4118.0±140.2±283.3	2804.3±171.0±225.4
4.5 – 5.0	3690.8±121.8±249.0	2611.4±153.9±187.4
5.0 – 5.5	3248.0±108.5±213.2	2013.2±133.7±151.5
5.5 – 6.0	2910.9± 96.5±193.3	1886.3±123.0±207.7
6.0 – 6.5	2381.8± 83.6±157.1	1610.8±105.5±129.0
6.5 – 7.0	1907.1± 70.2±126.9	1415.9± 93.2±112.7
7.0 – 7.5	1661.2± 63.4±119.0	1095.4± 76.5± 83.1
7.5 – 8.0	1364.5± 54.1± 96.8	910.1± 66.1± 74.4
8.0 – 8.5	1238.8± 49.7± 83.7	826.1± 60.3± 63.9
8.5 – 9.0	961.2± 41.8± 64.3	581.5± 50.7± 50.9
9.0 – 9.5	848.9± 38.4± 57.0	528.5± 44.7± 43.7
9.5 – 10.0	732.8± 34.6± 50.4	518.6± 43.0± 43.7
10.0 – 10.5	635.7± 30.9± 60.2	350.2± 33.9± 32.1
10.5 – 11.5	474.4± 18.4± 33.1	308.7± 21.6± 25.2
11.5 – 12.5	343.0± 14.7± 24.8	235.5± 18.0± 19.1
12.5 – 14.0	242.6± 10.2± 16.3	147.9± 11.1± 13.1
14.0 – 16.5	131.0± 5.6± 8.8	71.8± 5.7± 5.7
16.5 – 23.5	45.9± 1.9± 3.2	22.8± 1.9± 2.0
23.5 – 40.0	5.2± 0.4± 0.4	2.3± 0.4± 0.3

Table 6: Measured $B^{\pm}$ differential cross-sections (in units of nb) at 7 TeV and 13 TeV as functions of p_{T} in the range $2.0 < y < 4.5$. The cross-section ratio between 13 TeV and 7 TeV is also presented.

p_{T} [GeV/c]	7 TeV	13 TeV	$R(13/7)$
0.0 – 0.5	1163.5± 62.1±101.8	1949.2±187.7±182.4	1.68±0.18±0.17
0.5 – 1.0	3168.4± 99.0±237.0	5625.1±277.6±444.3	1.78±0.10±0.14
1.0 – 1.5	4664.6±108.1±383.1	9021.1±341.3±676.1	1.93±0.09±0.16
1.5 – 2.0	6150.2±118.6±459.3	11533.4±367.0±972.4	1.88±0.07±0.16
2.0 – 2.5	6708.3±117.1±566.0	12066.8±349.4±856.8	1.80±0.06±0.15
2.5 – 3.0	6896.7±110.2±454.0	13941.5±354.5±978.2	2.02±0.06±0.13
3.0 – 3.5	6850.5±108.2±442.2	13524.7±335.7±981.9	1.97±0.06±0.13
3.5 – 4.0	6561.5±103.2±462.6	12704.7±298.4±881.2	1.94±0.05±0.14
4.0 – 4.5	6004.1± 88.3±388.6	11586.5±277.0±794.5	1.93±0.05±0.12
4.5 – 5.0	5517.3± 82.8±338.2	11202.5±252.3±761.9	2.03±0.05±0.12
5.0 – 5.5	4899.1± 74.7±335.9	9625.0±215.4±628.0	1.96±0.05±0.13
5.5 – 6.0	4013.5± 60.5±238.5	8400.8±179.9±594.3	2.09±0.05±0.13
6.0 – 6.5	3578.6± 55.7±222.7	7274.4±154.2±494.3	2.03±0.05±0.13
6.5 – 7.0	2983.9± 45.5±189.6	6043.4±132.2±415.3	2.03±0.05±0.13
7.0 – 7.5	2491.0± 39.5±137.1	5198.3±113.2±369.3	2.09±0.06±0.13
7.5 – 8.0	2049.2± 33.3±141.3	4391.8± 98.3±297.9	2.14±0.06±0.15
8.0 – 8.5	1738.9± 28.6±104.5	4102.6± 92.0±286.4	2.36±0.07±0.15
8.5 – 9.0	1526.7± 26.2±104.5	3260.3± 77.2±233.3	2.14±0.06±0.16
9.0 – 9.5	1272.3± 22.8± 73.1	2750.5± 66.0±183.0	2.16±0.06±0.13
9.5 – 10.0	1038.1± 19.2± 62.6	2408.9± 58.2±160.6	2.32±0.07±0.14
10.0 – 10.5	909.9± 18.2± 65.8	2186.3± 53.0±148.1	2.40±0.08±0.18
10.5 – 11.5	736.8± 10.9± 51.2	1628.7± 30.6±113.0	2.21±0.05±0.16
11.5 – 12.5	516.2± 8.5± 32.7	1277.4± 26.0± 87.0	2.47±0.06±0.16
12.5 – 14.0	356.5± 5.4± 22.3	880.7± 16.1± 57.2	2.47±0.06±0.15
14.0 – 16.5	204.0± 3.0± 11.8	520.7± 9.0± 33.9	2.55±0.06±0.15
16.5 – 23.5	65.8± 0.9± 3.9	182.6± 2.9± 12.4	2.78±0.06±0.17
23.5 – 40.0	7.6± 0.2± 0.6	25.7± 0.6± 1.8	3.38±0.12±0.25

Table 7: Measured $B^{\pm}$ differential cross-sections (in units of μb) at 7 TeV and 13 TeV as functions of y in the p_{T} range $0 < p_{\mathrm{T}} < 40\,\mathrm{GeV}/c$. The cross-section ratio between 13 TeV and 7 TeV is also presented.

y	7 TeV	13 TeV	$R(13/7)$
2.0 – 2.5	23.5±0.3±2.0	45.6±0.8±3.6	1.94±0.04±0.19
2.5 – 3.0	22.1±0.1±1.4	43.1±0.4±2.9	1.95±0.02±0.12
3.0 – 3.5	18.2±0.1±1.0	36.4±0.3±2.4	2.00±0.02±0.10
3.5 – 4.0	13.4±0.1±0.8	28.9±0.3±1.9	2.16±0.02±0.12
4.0 – 4.5	8.8±0.1±0.6	19.3±0.4±1.4	2.21±0.05±0.16

References

[1] M. Cacciari, M. Greco, and P. Nason, *The p_{T} spectrum in heavy flavor hadroproduction*, JHEP **05** (1998) 007, `arXiv:hep-ph/9803400`.

[2] M. Cacciari, S. Frixione, and P. Nason, *The p_{T} spectrum in heavy flavor photoproduction*, JHEP **03** (2001) 006, `arXiv:hep-ph/0102134`.

[3] CMS collaboration, V. Khachatryan *et al.*, *Measurement of the B^+ production cross section in pp collisions at $\sqrt{s} = 7$ TeV*, Phys. Rev. Lett. **106** (2011) 112001, `arXiv:1101.0131`.

[4] CMS collaboration, V. Khachatryan *et al.*, *Measurement of the total and differential inclusive B^+ hadron cross sections in pp collisions at $\sqrt{s} = 13$ TeV*, Phys. Lett. **B771** (2017) 435, `arXiv:1609.00873`.

[5] ATLAS collaboration, G. Aad *et al.*, *Measurement of the differential cross-section of B^+ meson production in pp collisions at $\sqrt{s} = 7$ TeV at ATLAS*, JHEP **10** (2013) 042, `arXiv:1307.0126`.

[6] LHCb collaboration, R. Aaij *et al.*, *Measurement of the $B^{\pm}$ production cross-section in pp collisions at $\sqrt{s} = 7$ TeV*, JHEP **04** (2012) 093, `arXiv:1202.4812`.

[7] LHCb collaboration, R. Aaij *et al.*, *Measurement of B meson production cross-sections in proton-proton collisions at $\sqrt{s} = 7$ TeV*, JHEP **08** (2013) 117, `arXiv:1306.3663`.

[8] LHCb collaboration, A. A. Alves Jr. *et al.*, *The LHCb detector at the LHC*, JINST **3** (2008) S08005.

[9] LHCb collaboration, R. Aaij *et al.*, *LHCb detector performance*, Int. J. Mod. Phys. **A30** (2015) 1530022, `arXiv:1412.6352`.

[10] R. Aaij *et al.*, *The LHCb trigger and its performance in 2011*, JINST **8** (2013) P04022, `arXiv:1211.3055`.

[11] Particle Data Group, C. Patrignani *et al.*, *Review of particle physics*, Chin. Phys. **C40** (2016) 100001.

[12] T. Sjöstrand, S. Mrenna, and P. Skands, *A brief introduction to PYTHIA 8.1*, Comput. Phys. Commun. **178** (2008) 852, `arXiv:0710.3820`.

[13] I. Belyaev *et al.*, *Handling of the generation of primary events in Gauss, the LHCb simulation framework*, J. Phys. Conf. Ser. **331** (2011) 032047.

[14] D. J. Lange, *The EvtGen particle decay simulation package*, Nucl. Instrum. Meth. **A462** (2001) 152.

[15] P. Golonka and Z. Was, *PHOTOS Monte Carlo: A precision tool for QED corrections in Z and W decays*, Eur. Phys. J. **C45** (2006) 97, `arXiv:hep-ph/0506026`.

[16] Geant4 collaboration, J. Allison *et al.*, *Geant4 developments and applications*, IEEE Trans. Nucl. Sci. **53** (2006) 270; Geant4 collaboration, S. Agostinelli *et al.*, *Geant4: A simulation toolkit*, Nucl. Instrum. Meth. **A506** (2003) 250.

[17] M. Clemencic *et al.*, *The LHCb simulation application, Gauss: Design, evolution and experience*, J. Phys. Conf. Ser. **331** (2011) 032023.

[18] W. D. Hulsbergen, *Decay chain fitting with a Kalman filter*, Nucl. Instrum. Meth. **A552** (2005) 566, `arXiv:physics/0503191`.

[19] Belle collaboration, K. Abe *et al.*, *Measurement of branching fractions and charge asymmetries for two-body B meson decays with charmonium*, Phys. Rev. **D67** (2003) 032003, `arXiv:hep-ex/0211047`.

[20] BaBar collaboration, B. Aubert *et al.*, *Measurement of branching fractions and charge asymmetries for exclusive B decays to charmonium*, Phys. Rev. Lett. **94** (2005) 141801, `arXiv:hep-ex/0412062`.

[21] T. Skwarnicki, *A study of the radiative cascade transitions between the Upsilon-prime and Upsilon resonances*, PhD thesis, Institute of Nuclear Physics, Krakow, 1986, DESY-F31-86-02.

[22] O. Lupton, L. Anderlini, B. Sciascia, and V. Gligorov, *Calibration samples for particle identification at LHCb in Run 2*, LHCb-PUB-2016-005.

[23] LHCb collaboration, R. Aaij *et al.*, *Measurement of the track reconstruction efficiency at LHCb*, JINST **10** (2015) P02007, `arXiv:1408.1251`.

[24] LHCb collaboration, R. Aaij *et al.*, *Precision luminosity measurements at LHCb*, JINST **9** (2014) P12005, `arXiv:1410.0149`.

[25] D. Martínez Santos and F. Dupertuis, *Mass distributions marginalized over per-event errors*, Nucl. Instrum. Meth. **A764** (2014) 150, `arXiv:1312.5000`.

[26] M. Cacciari, M. L. Mangano, and P. Nason, *Gluon PDF constraints from the ratio of forward heavy-quark production at the LHC at* $\sqrt{s} = 7$ *and 13 TeV*, Eur. Phys. J. **C75** (2015) 610, `arXiv:1507.06197`.

LHCb collaboration

R. Aaij[40], B. Adeva[39], M. Adinolfi[48], Z. Ajaltouni[5], S. Akar[59], J. Albrecht[10], F. Alessio[40], M. Alexander[53], A. Alfonso Albero[38], S. Ali[43], G. Alkhazov[31], P. Alvarez Cartelle[55], A.A. Alves Jr[59], S. Amato[2], S. Amerio[23], Y. Amhis[7], L. An[3], L. Anderlini[18], G. Andreassi[41], M. Andreotti[17,g], J.E. Andrews[60], R.B. Appleby[56], F. Archilli[43], P. d'Argent[12], J. Arnau Romeu[6], A. Artamonov[37], M. Artuso[61], E. Aslanides[6], M. Atzeni[42], G. Auriemma[26], M. Baalouch[5], I. Babuschkin[56], S. Bachmann[12], J.J. Back[50], A. Badalov[38,m], C. Baesso[62], S. Baker[55], V. Balagura[7,b], W. Baldini[17], A. Baranov[35], R.J. Barlow[56], C. Barschel[40], S. Barsuk[7], W. Barter[56], F. Baryshnikov[32], V. Batozskaya[29], V. Battista[41], A. Bay[41], L. Beaucourt[4], J. Beddow[53], F. Bedeschi[24], I. Bediaga[1], A. Beiter[61], L.J. Bel[43], N. Beliy[63], V. Bellee[41], N. Belloli[21,i], K. Belous[37], I. Belyaev[32,40], E. Ben-Haim[8], G. Bencivenni[19], S. Benson[43], S. Beranek[9], A. Berezhnoy[33], R. Bernet[42], D. Berninghoff[12], E. Bertholet[8], A. Bertolin[23], C. Betancourt[42], F. Betti[15], M.-O. Bettler[40], M. van Beuzekom[43], Ia. Bezshyiko[42], S. Bifani[47], P. Billoir[8], A. Birnkraut[10], A. Bizzeti[18,u], M. Bjørn[57], T. Blake[50], F. Blanc[41], S. Blusk[61], V. Bocci[26], T. Boettcher[58], A. Bondar[36,w], N. Bondar[31], I. Bordyuzhin[32], S. Borghi[56], M. Borisyak[35], M. Borsato[39], F. Bossu[7], M. Boubdir[9], T.J.V. Bowcock[54], E. Bowen[42], C. Bozzi[17,40], S. Braun[12], T. Britton[61], J. Brodzicka[27], D. Brundu[16], E. Buchanan[48], C. Burr[56], A. Bursche[16,f], J. Buytaert[40], W. Byczynski[40], S. Cadeddu[16], H. Cai[64], R. Calabrese[17,g], R. Calladine[47], M. Calvi[21,i], M. Calvo Gomez[38,m], A. Camboni[38,m], P. Campana[19], D.H. Campora Perez[40], L. Capriotti[56], A. Carbone[15,e], G. Carboni[25,j], R. Cardinale[20,h], A. Cardini[16], P. Carniti[21,i], L. Carson[52], K. Carvalho Akiba[2], G. Casse[54], L. Cassina[21], M. Cattaneo[40], G. Cavallero[20,40,h], R. Cenci[24,t], D. Chamont[7], M.G. Chapman[48], M. Charles[8], Ph. Charpentier[40], G. Chatzikonstantinidis[47], M. Chefdeville[4], S. Chen[16], S.F. Cheung[57], S.-G. Chitic[40], V. Chobanova[39,40], M. Chrzaszcz[42,27], A. Chubykin[31], P. Ciambrone[19], X. Cid Vidal[39], G. Ciezarek[43], P.E.L. Clarke[52], M. Clemencic[40], H.V. Cliff[49], J. Closier[40], J. Cogan[6], E. Cogneras[5], V. Cogoni[16,f], L. Cojocariu[30], P. Collins[40], T. Colombo[40], A. Comerma-Montells[12], A. Contu[40], A. Cook[48], G. Coombs[40], S. Coquereau[38], G. Corti[40], M. Corvo[17,g], C.M. Costa Sobral[50], B. Couturier[40], G.A. Cowan[52], D.C. Craik[58], A. Crocombe[50], M. Cruz Torres[1], R. Currie[52], C. D'Ambrosio[40], F. Da Cunha Marinho[2], E. Dall'Occo[43], J. Dalseno[48], A. Davis[3], O. De Aguiar Francisco[40], S. De Capua[56], M. De Cian[12], J.M. De Miranda[1], L. De Paula[2], M. De Serio[14,d], P. De Simone[19], C.T. Dean[53], D. Decamp[4], L. Del Buono[8], H.-P. Dembinski[11], M. Demmer[10], A. Dendek[28], D. Derkach[35], O. Deschamps[5], F. Dettori[54], B. Dey[65], A. Di Canto[40], P. Di Nezza[19], H. Dijkstra[40], F. Dordei[40], M. Dorigo[40], A. Dosil Suárez[39], L. Douglas[53], A. Dovbnya[45], K. Dreimanis[54], L. Dufour[43], G. Dujany[8], P. Durante[40], R. Dzhelyadin[37], M. Dziewiecki[12], A. Dziurda[40], A. Dzyuba[31], S. Easo[51], M. Ebert[52], U. Egede[55], V. Egorychev[32], S. Eidelman[36,w], S. Eisenhardt[52], U. Eitschberger[10], R. Ekelhof[10], L. Eklund[53], S. Ely[61], S. Esen[12], H.M. Evans[49], T. Evans[57], A. Falabella[15], N. Farley[47], S. Farry[54], D. Fazzini[21,i], L. Federici[25], D. Ferguson[52], G. Fernandez[38], P. Fernandez Declara[40], A. Fernandez Prieto[39], F. Ferrari[15], F. Ferreira Rodrigues[2], M. Ferro-Luzzi[40], S. Filippov[34], R.A. Fini[14], M. Fiorini[17,g], M. Firlej[28], C. Fitzpatrick[41], T. Fiutowski[28], F. Fleuret[7,b], K. Fohl[40], M. Fontana[16,40], F. Fontanelli[20,h], D.C. Forshaw[61], R. Forty[40], V. Franco Lima[54], M. Frank[40], C. Frei[40], J. Fu[22,q], W. Funk[40], E. Furfaro[25,j], C. Färber[40], E. Gabriel[52], A. Gallas Torreira[39], D. Galli[15,e], S. Gallorini[23], S. Gambetta[52], M. Gandelman[2], P. Gandini[22], Y. Gao[3], L.M. Garcia Martin[70], J. García Pardiñas[39], J. Garra Tico[49], L. Garrido[38], P.J. Garsed[49], D. Gascon[38], C. Gaspar[40], L. Gavardi[10], G. Gazzoni[5], D. Gerick[12], E. Gersabeck[56], M. Gersabeck[56], T. Gershon[50], Ph. Ghez[4], S. Gianì[41], V. Gibson[49], O.G. Girard[41], L. Giubega[30], K. Gizdov[52], V.V. Gligorov[8], D. Golubkov[32], A. Golutvin[55], A. Gomes[1,a], I.V. Gorelov[33], C. Gotti[21,i], E. Govorkova[43], J.P. Grabowski[12], R. Graciani Diaz[38], L.A. Granado Cardoso[40], E. Graugés[38], E. Graverini[42],

G. Graziani[18], A. Grecu[30], R. Greim[9], P. Griffith[16], L. Grillo[21], L. Gruber[40],
B.R. Gruberg Cazon[57], O. Grünberg[67], E. Gushchin[34], Yu. Guz[37], T. Gys[40], C. Göbel[62],
T. Hadavizadeh[57], C. Hadjivasiliou[5], G. Haefeli[41], C. Haen[40], S.C. Haines[49], B. Hamilton[60],
X. Han[12], T.H. Hancock[57], S. Hansmann-Menzemer[12], N. Harnew[57], S.T. Harnew[48], C. Hasse[40],
M. Hatch[40], J. He[63], M. Hecker[55], K. Heinicke[10], A. Heister[9], K. Hennessy[54], P. Henrard[5],
L. Henry[70], E. van Herwijnen[40], M. Heß[67], A. Hicheur[2], D. Hill[57], C. Hombach[56],
P.H. Hopchev[41], W. Hu[65], Z.C. Huard[59], W. Hulsbergen[43], T. Humair[55], M. Hushchyn[35],
D. Hutchcroft[54], P. Ibis[10], M. Idzik[28], P. Ilten[58], R. Jacobsson[40], J. Jalocha[57], E. Jans[43],
A. Jawahery[60], F. Jiang[3], M. John[57], D. Johnson[40], C.R. Jones[49], C. Joram[40], B. Jost[40],
N. Jurik[57], S. Kandybei[45], M. Karacson[40], J.M. Kariuki[48], S. Karodia[53], N. Kazeev[35],
M. Kecke[12], F. Keizer[49], M. Kelsey[61], M. Kenzie[49], T. Ketel[44], E. Khairullin[35], B. Khanji[12],
C. Khurewathanakul[41], T. Kirn[9], S. Klaver[56], K. Klimaszewski[29], T. Klimkovich[11], S. Koliiev[46],
M. Kolpin[12], R. Kopecna[12], P. Koppenburg[43], A. Kosmyntseva[32], S. Kotriakhova[31],
M. Kozeiha[5], L. Kravchuk[34], M. Kreps[50], F. Kress[55], P. Krokovny[36,w], F. Kruse[10],
W. Krzemien[29], W. Kucewicz[27,l], M. Kucharczyk[27], V. Kudryavtsev[36,w], A.K. Kuonen[41],
T. Kvaratskheliya[32,40], D. Lacarrere[40], G. Lafferty[56], A. Lai[16], G. Lanfranchi[19],
C. Langenbruch[9], T. Latham[50], C. Lazzeroni[47], R. Le Gac[6], A. Leflat[33,40], J. Lefrançois[7],
R. Lefèvre[5], F. Lemaitre[40], E. Lemos Cid[39], O. Leroy[6], T. Lesiak[27], B. Leverington[12], P.-R. Li[63],
T. Li[3], Y. Li[7], Z. Li[61], T. Likhomanenko[68], R. Lindner[40], F. Lionetto[42], V. Lisovskyi[7], X. Liu[3],
D. Loh[50], A. Loi[16], I. Longstaff[53], J.H. Lopes[2], D. Lucchesi[23,o], M. Lucio Martinez[39], H. Luo[52],
A. Lupato[23], E. Luppi[17,g], O. Lupton[40], A. Lusiani[24], X. Lyu[63], F. Machefert[7], F. Maciuc[30],
V. Macko[41], P. Mackowiak[10], S. Maddrell-Mander[48], O. Maev[31,40], K. Maguire[56],
D. Maisuzenko[31], M.W. Majewski[28], S. Malde[57], B. Malecki[27], A. Malinin[68], T. Maltsev[36,w],
G. Manca[16,f], G. Mancinelli[6], D. Marangotto[22,q], J. Maratas[5,v], J.F. Marchand[4], U. Marconi[15],
C. Marin Benito[38], M. Marinangeli[41], P. Marino[41], J. Marks[12], G. Martellotti[26], M. Martin[6],
M. Martinelli[41], D. Martinez Santos[39], F. Martinez Vidal[70], L.M. Massacrier[7], A. Massafferri[1],
R. Matev[40], A. Mathad[50], Z. Mathe[40], C. Matteuzzi[21], A. Mauri[42], E. Maurice[7,b], B. Maurin[41],
A. Mazurov[47], M. McCann[55,40], A. McNab[56], R. McNulty[13], J.V. Mead[54], B. Meadows[59],
C. Meaux[6], F. Meier[10], N. Meinert[67], D. Melnychuk[29], M. Merk[43], A. Merli[22,40,q],
E. Michielin[23], D.A. Milanes[66], E. Millard[50], M.-N. Minard[4], L. Minzoni[17], D.S. Mitzel[12],
A. Mogini[8], J. Molina Rodriguez[1], T. Mombächer[10], I.A. Monroy[66], S. Monteil[5],
M. Morandin[23], M.J. Morello[24,t], O. Morgunova[68], J. Moron[28], A.B. Morris[52], R. Mountain[61],
F. Muheim[52], M. Mulder[43], D. Müller[56], J. Müller[10], K. Müller[42], V. Müller[10], P. Naik[48],
T. Nakada[41], R. Nandakumar[51], A. Nandi[57], I. Nasteva[2], M. Needham[52], N. Neri[22,40],
S. Neubert[12], N. Neufeld[40], M. Neuner[12], T.D. Nguyen[41], C. Nguyen-Mau[41,n], S. Nieswand[9],
R. Niet[10], N. Nikitin[33], T. Nikodem[12], A. Nogay[68], D.P. O'Hanlon[50], A. Oblakowska-Mucha[28],
V. Obraztsov[37], S. Ogilvy[19], R. Oldeman[16,f], C.J.G. Onderwater[71], A. Ossowska[27],
J.M. Otalora Goicochea[2], P. Owen[42], A. Oyanguren[70], P.R. Pais[41], A. Palano[14],
M. Palutan[19,40], A. Papanestis[51], M. Pappagallo[14,d], L.L. Pappalardo[17,g], W. Parker[60],
C. Parkes[56], G. Passaleva[18,40], A. Pastore[14,d], M. Patel[55], C. Patrignani[15,e], A. Pearce[40],
A. Pellegrino[43], G. Penso[26], M. Pepe Altarelli[40], S. Perazzini[40], P. Perret[5], L. Pescatore[41],
K. Petridis[48], A. Petrolini[20,h], A. Petrov[68], M. Petruzzo[22,q], E. Picatoste Olloqui[38],
B. Pietrzyk[4], M. Pikies[27], D. Pinci[26], F. Pisani[40], A. Pistone[20,h], A. Piucci[12], V. Placinta[30],
S. Playfer[52], M. Plo Casasus[39], F. Polci[8], M. Poli Lener[19], A. Poluektov[50], I. Polyakov[61],
E. Polycarpo[2], G.J. Pomery[48], S. Ponce[40], A. Popov[37], D. Popov[11,40], S. Poslavskii[37],
C. Potterat[2], E. Price[48], J. Prisciandaro[39], C. Prouve[48], V. Pugatch[46], A. Puig Navarro[42],
H. Pullen[57], G. Punzi[24,p], W. Qian[50], R. Quagliani[7,48], B. Quintana[5], B. Rachwal[28],
J.H. Rademacker[48], M. Rama[24], M. Ramos Pernas[39], M.S. Rangel[2], I. Raniuk[45,†],
F. Ratnikov[35], G. Raven[44], M. Ravonel Salzgeber[40], M. Reboud[4], F. Redi[55], S. Reichert[10],
A.C. dos Reis[1], C. Remon Alepuz[70], V. Renaudin[7], S. Ricciardi[51], S. Richards[48], M. Rihl[40],

K. Rinnert[54], V. Rives Molina[38], P. Robbe[7], A. Robert[8], A.B. Rodrigues[1], E. Rodrigues[59], J.A. Rodriguez Lopez[66], A. Rogozhnikov[35], S. Roiser[40], A. Rollings[57], V. Romanovskiy[37], A. Romero Vidal[39], J.W. Ronayne[13], M. Rotondo[19], M.S. Rudolph[61], T. Ruf[40], P. Ruiz Valls[70], J. Ruiz Vidal[70], J.J. Saborido Silva[39], E. Sadykhov[32], N. Sagidova[31], B. Saitta[16,f], V. Salustino Guimaraes[62], C. Sanchez Mayordomo[70], B. Sanmartin Sedes[39], R. Santacesaria[26], C. Santamarina Rios[39], M. Santimaria[19], E. Santovetti[25,j], G. Sarpis[56], A. Sarti[19,k], C. Satriano[26,s], A. Satta[25], D.M. Saunders[48], D. Savrina[32,33], S. Schael[9], M. Schellenberg[10], M. Schiller[53], H. Schindler[40], M. Schmelling[11], T. Schmelzer[10], B. Schmidt[40], O. Schneider[41], A. Schopper[40], H.F. Schreiner[59], M. Schubiger[41], M.-H. Schune[7], R. Schwemmer[40], B. Sciascia[19], A. Sciubba[26,k], A. Semennikov[32], E.S. Sepulveda[8], A. Sergi[47], N. Serra[42], J. Serrano[6], L. Sestini[23], P. Seyfert[40], M. Shapkin[37], I. Shapoval[45], Y. Shcheglov[31], T. Shears[54], L. Shekhtman[36,w], V. Shevchenko[68], B.G. Siddi[17], R. Silva Coutinho[42], L. Silva de Oliveira[2], G. Simi[23,o], S. Simone[14,d], M. Sirendi[49], N. Skidmore[48], T. Skwarnicki[61], E. Smith[55], I.T. Smith[52], J. Smith[49], M. Smith[55], l. Soares Lavra[1], M.D. Sokoloff[59], F.J.P. Soler[53], B. Souza De Paula[2], B. Spaan[10], P. Spradlin[53], S. Sridharan[40], F. Stagni[40], M. Stahl[12], S. Stahl[40], P. Stefko[41], S. Stefkova[55], O. Steinkamp[42], S. Stemmle[12], O. Stenyakin[37], M. Stepanova[31], H. Stevens[10], S. Stone[61], B. Storaci[42], S. Stracka[24,p], M.E. Stramaglia[41], M. Straticiuc[30], U. Straumann[42], J. Sun[3], L. Sun[64], W. Sutcliffe[55], K. Swientek[28], V. Syropoulos[44], T. Szumlak[28], M. Szymanski[63], S. T'Jampens[4], A. Tayduganov[6], T. Tekampe[10], G. Tellarini[17,g], F. Teubert[40], E. Thomas[40], J. van Tilburg[43], M.J. Tilley[55], V. Tisserand[4], M. Tobin[41], S. Tolk[49], L. Tomassetti[17,g], D. Tonelli[24], F. Toriello[61], R. Tourinho Jadallah Aoude[1], E. Tournefier[4], M. Traill[53], M.T. Tran[41], M. Tresch[42], A. Trisovic[40], A. Tsaregorodtsev[6], P. Tsopelas[43], A. Tully[49], N. Tuning[43,40], A. Ukleja[29], A. Usachov[7], A. Ustyuzhanin[35], U. Uwer[12], C. Vacca[16,f], A. Vagner[69], V. Vagnoni[15,40], A. Valassi[40], S. Valat[40], G. Valenti[15], R. Vazquez Gomez[40], P. Vazquez Regueiro[39], S. Vecchi[17], M. van Veghel[43], J.J. Velthuis[48], M. Veltri[18,r], G. Veneziano[57], A. Venkateswaran[61], T.A. Verlage[9], M. Vernet[5], M. Vesterinen[57], J.V. Viana Barbosa[40], B. Viaud[7], D. Vieira[63], M. Vieites Diaz[39], H. Viemann[67], X. Vilasis-Cardona[38,m], M. Vitti[49], V. Volkov[33], A. Vollhardt[42], B. Voneki[40], A. Vorobyev[31], V. Vorobyev[36,w], C. Voß[9], J.A. de Vries[43], C. Vázquez Sierra[39], R. Waldi[67], C. Wallace[50], R. Wallace[13], J. Walsh[24], J. Wang[61], D.R. Ward[49], H.M. Wark[54], N.K. Watson[47], D. Websdale[55], A. Weiden[42], C. Weisser[58], M. Whitehead[40], J. Wicht[50], G. Wilkinson[57], M. Wilkinson[61], M. Williams[56], M.P. Williams[47], M. Williams[58], T. Williams[47], F.F. Wilson[51,40], J. Wimberley[60], M. Winn[7], J. Wishahi[10], W. Wislicki[29], M. Witek[27], G. Wormser[7], S.A. Wotton[49], K. Wraight[53], K. Wyllie[40], Y. Xie[65], M. Xu[65], Z. Xu[4], Z. Yang[3], Z. Yang[60], Y. Yao[61], H. Yin[65], J. Yu[65], X. Yuan[61], O. Yushchenko[37], K.A. Zarebski[47], M. Zavertyaev[11,c], L. Zhang[3], Y. Zhang[7], A. Zhelezov[12], Y. Zheng[63], X. Zhu[3], V. Zhukov[33], J.B. Zonneveld[52], S. Zucchelli[15].

[1]*Centro Brasileiro de Pesquisas Físicas (CBPF), Rio de Janeiro, Brazil*
[2]*Universidade Federal do Rio de Janeiro (UFRJ), Rio de Janeiro, Brazil*
[3]*Center for High Energy Physics, Tsinghua University, Beijing, China*
[4]*LAPP, Université Savoie Mont-Blanc, CNRS/IN2P3, Annecy-Le-Vieux, France*
[5]*Clermont Université, Université Blaise Pascal, CNRS/IN2P3, LPC, Clermont-Ferrand, France*
[6]*Aix Marseille Univ, CNRS/IN2P3, CPPM, Marseille, France*
[7]*LAL, Université Paris-Sud, CNRS/IN2P3, Orsay, France*
[8]*LPNHE, Université Pierre et Marie Curie, Université Paris Diderot, CNRS/IN2P3, Paris, France*
[9]*I. Physikalisches Institut, RWTH Aachen University, Aachen, Germany*
[10]*Fakultät Physik, Technische Universität Dortmund, Dortmund, Germany*
[11]*Max-Planck-Institut für Kernphysik (MPIK), Heidelberg, Germany*
[12]*Physikalisches Institut, Ruprecht-Karls-Universität Heidelberg, Heidelberg, Germany*
[13]*School of Physics, University College Dublin, Dublin, Ireland*
[14]*Sezione INFN di Bari, Bari, Italy*

[15]*Sezione INFN di Bologna, Bologna, Italy*
[16]*Sezione INFN di Cagliari, Cagliari, Italy*
[17]*Universita e INFN, Ferrara, Ferrara, Italy*
[18]*Sezione INFN di Firenze, Firenze, Italy*
[19]*Laboratori Nazionali dell'INFN di Frascati, Frascati, Italy*
[20]*Sezione INFN di Genova, Genova, Italy*
[21]*Universita & INFN, Milano-Bicocca, Milano, Italy*
[22]*Sezione di Milano, Milano, Italy*
[23]*Sezione INFN di Padova, Padova, Italy*
[24]*Sezione INFN di Pisa, Pisa, Italy*
[25]*Sezione INFN di Roma Tor Vergata, Roma, Italy*
[26]*Sezione INFN di Roma La Sapienza, Roma, Italy*
[27]*Henryk Niewodniczanski Institute of Nuclear Physics Polish Academy of Sciences, Kraków, Poland*
[28]*AGH - University of Science and Technology, Faculty of Physics and Applied Computer Science, Kraków, Poland*
[29]*National Center for Nuclear Research (NCBJ), Warsaw, Poland*
[30]*Horia Hulubei National Institute of Physics and Nuclear Engineering, Bucharest-Magurele, Romania*
[31]*Petersburg Nuclear Physics Institute (PNPI), Gatchina, Russia*
[32]*Institute of Theoretical and Experimental Physics (ITEP), Moscow, Russia*
[33]*Institute of Nuclear Physics, Moscow State University (SINP MSU), Moscow, Russia*
[34]*Institute for Nuclear Research of the Russian Academy of Sciences (INR RAN), Moscow, Russia*
[35]*Yandex School of Data Analysis, Moscow, Russia*
[36]*Budker Institute of Nuclear Physics (SB RAS), Novosibirsk, Russia*
[37]*Institute for High Energy Physics (IHEP), Protvino, Russia*
[38]*ICCUB, Universitat de Barcelona, Barcelona, Spain*
[39]*Universidad de Santiago de Compostela, Santiago de Compostela, Spain*
[40]*European Organization for Nuclear Research (CERN), Geneva, Switzerland*
[41]*Institute of Physics, Ecole Polytechnique Fédérale de Lausanne (EPFL), Lausanne, Switzerland*
[42]*Physik-Institut, Universität Zürich, Zürich, Switzerland*
[43]*Nikhef National Institute for Subatomic Physics, Amsterdam, The Netherlands*
[44]*Nikhef National Institute for Subatomic Physics and VU University Amsterdam, Amsterdam, The Netherlands*
[45]*NSC Kharkiv Institute of Physics and Technology (NSC KIPT), Kharkiv, Ukraine*
[46]*Institute for Nuclear Research of the National Academy of Sciences (KINR), Kyiv, Ukraine*
[47]*University of Birmingham, Birmingham, United Kingdom*
[48]*H.H. Wills Physics Laboratory, University of Bristol, Bristol, United Kingdom*
[49]*Cavendish Laboratory, University of Cambridge, Cambridge, United Kingdom*
[50]*Department of Physics, University of Warwick, Coventry, United Kingdom*
[51]*STFC Rutherford Appleton Laboratory, Didcot, United Kingdom*
[52]*School of Physics and Astronomy, University of Edinburgh, Edinburgh, United Kingdom*
[53]*School of Physics and Astronomy, University of Glasgow, Glasgow, United Kingdom*
[54]*Oliver Lodge Laboratory, University of Liverpool, Liverpool, United Kingdom*
[55]*Imperial College London, London, United Kingdom*
[56]*School of Physics and Astronomy, University of Manchester, Manchester, United Kingdom*
[57]*Department of Physics, University of Oxford, Oxford, United Kingdom*
[58]*Massachusetts Institute of Technology, Cambridge, MA, United States*
[59]*University of Cincinnati, Cincinnati, OH, United States*
[60]*University of Maryland, College Park, MD, United States*
[61]*Syracuse University, Syracuse, NY, United States*
[62]*Pontifícia Universidade Católica do Rio de Janeiro (PUC-Rio), Rio de Janeiro, Brazil, associated to* [2]
[63]*University of Chinese Academy of Sciences, Beijing, China, associated to* [3]
[64]*School of Physics and Technology, Wuhan University, Wuhan, China, associated to* [3]
[65]*Institute of Particle Physics, Central China Normal University, Wuhan, Hubei, China, associated to* [3]
[66]*Departamento de Fisica , Universidad Nacional de Colombia, Bogota, Colombia, associated to* [8]
[67]*Institut für Physik, Universität Rostock, Rostock, Germany, associated to* [12]
[68]*National Research Centre Kurchatov Institute, Moscow, Russia, associated to* [32]

[69]*National Research Tomsk Polytechnic University, Tomsk, Russia, associated to* [32]
[70]*Instituto de Fisica Corpuscular, Centro Mixto Universidad de Valencia - CSIC, Valencia, Spain, associated to* [38]
[71]*Van Swinderen Institute, University of Groningen, Groningen, The Netherlands, associated to* [43]

[a]*Universidade Federal do Triângulo Mineiro (UFTM), Uberaba-MG, Brazil*
[b]*Laboratoire Leprince-Ringuet, Palaiseau, France*
[c]*P.N. Lebedev Physical Institute, Russian Academy of Science (LPI RAS), Moscow, Russia*
[d]*Università di Bari, Bari, Italy*
[e]*Università di Bologna, Bologna, Italy*
[f]*Università di Cagliari, Cagliari, Italy*
[g]*Università di Ferrara, Ferrara, Italy*
[h]*Università di Genova, Genova, Italy*
[i]*Università di Milano Bicocca, Milano, Italy*
[j]*Università di Roma Tor Vergata, Roma, Italy*
[k]*Università di Roma La Sapienza, Roma, Italy*
[l]*AGH - University of Science and Technology, Faculty of Computer Science, Electronics and Telecommunications, Kraków, Poland*
[m]*LIFAELS, La Salle, Universitat Ramon Llull, Barcelona, Spain*
[n]*Hanoi University of Science, Hanoi, Viet Nam*
[o]*Università di Padova, Padova, Italy*
[p]*Università di Pisa, Pisa, Italy*
[q]*Università degli Studi di Milano, Milano, Italy*
[r]*Università di Urbino, Urbino, Italy*
[s]*Università della Basilicata, Potenza, Italy*
[t]*Scuola Normale Superiore, Pisa, Italy*
[u]*Università di Modena e Reggio Emilia, Modena, Italy*
[v]*Iligan Institute of Technology (IIT), Iligan, Philippines*
[w]*Novosibirsk State University, Novosibirsk, Russia*

[†]*Deceased*